three. Indeed, when v_3/v_2 drops below the $\Delta+2\sigma$ contour line, in figure 4.a, the other Higgses start to contribute and L^+L^- production increases by a factor of $\mathcal{O}(10)$, for $m_L \lesssim \mathcal{O}(100)GeV$.

It should also be pointed that, for $MSSM$ model parameters which yield a particle spectrum similar (*i.e.*, with comparable masses) to that of E_6, a fair chunk of its parameter space is eliminated by unitarity constraints.[7] In particular, for the results shown in figure 5.a, $MSSM$ production is restricted to the region $m_L \lesssim \mathcal{O}(250)GeV$, for $m_{H_1^0} \gtrsim \mathcal{O}(600)GeV$ and $\tan\beta \lesssim \mathcal{O}(5)$. For more conservative $MSSM$ parameters, $m_L \lesssim \mathcal{O}(400)GeV$.

3 Closing Remarks

A simple E_6 model was constructed and used to compute L^+L^- production at high energy hadron colliders. We expect $\mathcal{O}(10^{4\pm1})events/yr$ at LHC and "zero" at the TEVATRON, for $50GeV \leq m_L \leq 600GeV$. The results were a factor of at least 10 less than the $MSSM$ results due to the CDF and $D\emptyset$ soft-limits on m_{Z_2},[11] which caused the $H^0_{1,2}$ and P^0 contributions to become suppressed.

Acknowledgments

This research was funded by $NSERC$ of Canada and $FCAR$ du Quebec.

References

1. M.M. Boyce, *String Inspired QCD and E_6 Models*, Ph.D. thesis (1996), Carleton U., Dept. of Physics, 1125 Colonel By Dr., Ottawa, ONT, Canada, K1S-5B6.
2. M.M. Boyce, M.A. Doncheski, and H. König, work in progress.[1]
3. JoAnne L. Hewett and Thomas G. Rizzo, *Phys. Rep.* **183**, 193 (1989).
4. J. Ellis, *et al.*, *Nucl. Phys.* B **276**, 14 (1986)
5. H.E. Haber and G.L. Kane, *Phys. Rep.* **117**, 72 (1985).
6. C.N. Yang, *Phys. Rev.* D **77**, 242 (1950).
7. J.E. Cieza Montalvo, *et al.*, *Phys. Rev.* D **46**, 181 (1992).
8. Particle Data Group, *Phys. Rev.* D **50**, 1173 (1994).
9. John Ellis, K. Enqvist, *et al.*, *Mod. Phys. Lett.* A **1**, 57 (1986).
10. J.F. Gunion, *et al.*, *Phys. Rev.* D **28**, 105 (1988)
11. Melvyn J. Shochet, *Physics At The Fermilab Collider, The Albuquerque Meeting, Aug. 2-6, 1994*, ed. Sally Seidel (World Scientific 1994).
12. D. Duke and J. Owens, *Phys. Rev.* D **30**, 49 (1984).
    J. Owens, *Phys. Lett.* B **266**, 126 (1991).

in MULTISCALE PHENOMENA AND THEIR SIMULATION
PROC. of INTERNATIONAL CONFERENCE, BIELEFELD 1996
Eds B. MONIEN, F. KARSCH and H. SATZ

THE ELASTIC PROPERTIES OF A FLAT CRYSTALLINE MEMBRANE

MARK BOWICK, SIMON CATTERALL, MARCO FALCIONI
GUDMAR THORLEIFSSON
Department of Physics, Syracuse University
Syracuse, NY 13244-1130, USA

KOSTANTINOS ANAGOSTOPOULOS
The Niels Bohr Institute
Blegdamsvej 17, DK-2100 Copenhagen Ø, Denmark

We investigate a simple model of a crystalline surface with bending rigidity using Monte Carlo simulations. We focus our study on the flat phase of the model and measure its elastic properties. This model does not include any bare elastic constants, which are necessary to understand the stability of the flat phase in a theoretical framework. Yet, we come to the remarkable conclusion that this model has a stable flat phase. This phase is in the same universality class as the flat phase of other models of crystalline surfaces which explicitly incorporate elastic constants. The value of the roughness exponent, measured at bending rigidity $\kappa = 1.1$, is $\zeta = 0.64(2)$.

1 Introduction

A crystalline surface is a 2-dimensional structure with fixed connectivity, embedded in a 3-dimensional space. This means that particles that compose the surface are connected to their neighbors by un-breakable bonds. Also known as polymerized or tethered membranes, crystalline surfaces appear naturally in many different physical systems. They are expected to have an interesting phase structure, with a high temperature crumpled phase and a low temperature ordered or flat phase.[1]

Inorganic examples of crystalline surfaces are thin sheets of graphite-oxide in aqueous suspension[2] and the rag-like structures found in MoS_2.[3] There are also biological examples of crystalline membranes, such as the spectrin skeleton of red blood cells. This is a triangulated 2-dimensional structure made up of vertices (actin oligomers) and edges (spectrin tetramers), with about 70,000 plaquettes. Crystalline membranes can also be synthesized in the laboratory by polymerizing amphiphillic monolayers or bilayers.[1]

In recent years there has been a lot of interest in crystalline surfaces. Both analytical and numerical tools have become available and provided a picture of their phase diagram. There is compelling evidence that models of non self-avoiding (phantom) crystalline surfaces have a second order phase transition

(the crumpling transition) separating a crumpled and a flat phase. The inclusion of self-avoidance in the models, which clearly is present in real systems, does not change the behavior of the models in the flat phase.

In addition to biological examples, surfaces arise naturally in string theory. In the Euclidean formulation, the Polyakov action for a bosonic string describes a 2-dimensional world-sheet embedded in d-dimensions, where d is the number of non-compact bosonic fields.[7] A lot of work has been done to understand crystalline and random (fluid) surfaces embedded in $\mathbb{R}^3$ with extrinsic curvature as a discretized model for strings. The models used in this context are rather different, and simpler, than their condensed-matter counterparts, since they do not include elastic constants.[6]

The motivation of the work presented in this talk is to understand whether such a simple model of a phantom crystalline surface is indeed capable of describing a real polymerized membrane in the flat phase. Using numerical simulations we want to demonstrate that the elastic properties of this model agree with the analytical and experimental results on polymerized membranes.

2 Continuous Models of Surfaces

Usually a crystalline elastic membrane is characterized by its bending rigidity, its shear modulus, and its compression modulus. If a membrane is thin with respect to its lateral extension, it can be described by a purely 2-dimensional surface embedded in $\mathbb{R}^3$. We introduce a set of intrinsic coordinates (x_1, x_2) and write a continuous Hamiltonian for an asymptotically flat fixed-connectivity surface in the Monge gauge:

$$H = \frac{\kappa}{2} \int d^2x \left[\left(\partial^2 h\right)^2 + \mu (u_{ij})^2 + \frac{\lambda}{2} (u_{ii})^2 \right] \tag{1}$$

where

$$u_{ij} = \frac{1}{2} \left(\partial_i \mathbf{r} \cdot \partial_j \mathbf{r} - \delta_{ij} \right) \simeq \frac{1}{2} \left(\partial_i u_j + \partial_j u_i \right) + \left(\partial_i h \right) \left(\partial_j h \right) \tag{2}$$

is the stress tensor, which vanishes at $T = 0$, μ and λ are the Lamé coefficients and κ is the bending rigidity. The Monge gauge is a natural parameterization for a nearly flat surface (no over-hangs):

$$\mathbf{r} = \mathbf{x} + \mathbf{u} + h\hat{z} \tag{3}$$

where $\mathbf{x}$ is the equilibrium position of the surface, assumed to lie in the $\hat{x}$-$\hat{y}$ plane, $\mathbf{u}$ is the strain, or in-plane deformation, and h is the out-of-plane deformation.

There have been extensive analytical studies of the action Eq. (1). The crucial result, obtained in a self-consistent screening approximation,[13] is that at large wavelength the coupling constants κ, λ and μ acquire an anomalous scaling dimension,

$$\kappa_R(q) \sim q^{-\eta} \text{ and } \lambda \sim \mu \sim q^{\eta_u}, \tag{4}$$

where η and η_u are related by $\eta = 1 - \eta_u/2$. A renormalization group analysis indicates that the bending rigidity stiffens at long wavelength while the elastic constants soften. This result can be understood naively by comparing a flat sheet of paper to a sheet which has been crumpled and then unfolded: the flat paper is very flexible but not at all stretchable; the crumpled paper is much harder to bend, but can be stretched.

3 Discretized Models of Surfaces

The usual discretized analogue of Eq. (1) is a tethering pair potential and a bending energy term. Commonly used pair potential include explicitly shear and compression moduli, and bending rigidity, corresponding to λ, μ and κ.[6] We are interested in a much simpler model: consider N particles laid out in a 2-dimensional triangular lattice. $\mathbf{r}_i$ is the position of the particle i, and $\mathbf{n}_\alpha$ is the normal to the triangle α. The action is

$$\mathcal{H} = \sum_{\langle ij \rangle} (\mathbf{r}_i - \mathbf{r}_j)^2 - \kappa \sum_{\langle \alpha\beta \rangle} \mathbf{n}_\alpha \cdot \mathbf{n}_\beta, \tag{5}$$

where the sums extend only to nearest neighbors and κ is the bending rigidity. In this case the tethering potential is a simple Gaussian term, which does not prevent the surface from shrinking. The bare elastic constants (or Lamé coefficients) are not included. In fact, the first term is simply the discretization of $\partial\mathbf{r}\partial\mathbf{r}$. A great deal of effort has gone in understanding the crumpling transition that this model exhibits.[8,9] It is our goal to show that this model has a stable flat phase which corresponds to the continuous Hamiltonian of Eq. (1).

Since we are interested in the flat phase we study surfaces with *free boundaries*. Mainly for technical reasons, we choose a surface with rhomboidal shape. We do not include self avoidance as it is irrelevant in the flat phase.

4 Numerical Simulations and Observables

To understand the behavior of a system at thermal equilibrium we must evaluate the partition function

$$\mathcal{Z} = \int [d\mathbf{r}] \exp(-\beta H[\mathbf{r}]) \tag{6}$$

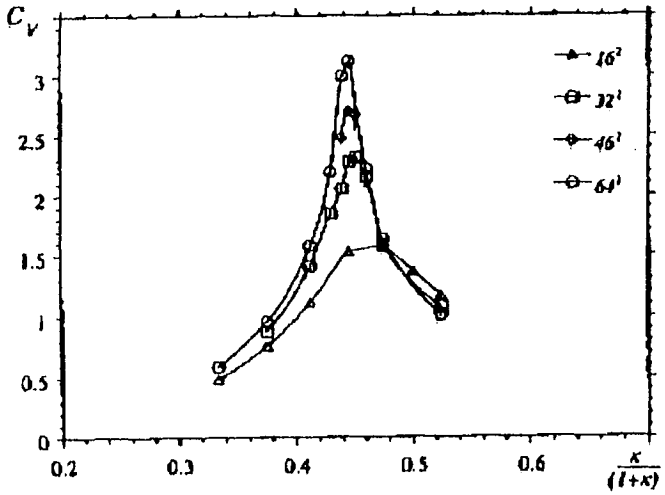

Figure 1: The specific heat versus the reduced variable $\kappa/(1+\kappa)$

and calculate observables O

$$\langle O \rangle = \frac{1}{Z} \int [d\mathbf{r}]\, O[\mathbf{r}] \exp(-\beta H[\mathbf{r}]). \tag{7}$$

We use Monte Carlo methods to evaluate the integral and to measure the observables.

4.1 The specific heat

As we are interested in the flat phase of the model we need to locate the phase transition. This can be done by measuring the specific heat

$$C_V = \frac{3(N-1)}{2} + \frac{\kappa^2}{3N}(\langle S_c^2 \rangle - \langle S_c \rangle^2), \tag{8}$$

where N is the number of particles and S_c is the bending energy term in the Hamiltonian (1). Previous numerical studies have shown that this model has a second-order phase transition at a critical value of the bending rigidity κ_c, where the specific heat diverges as

$$C_V \sim |\kappa - \kappa_c|^{-\alpha}. \tag{9}$$

α is a *critical exponent*. For a system of finite size the expression Eq. (7) can not be singular. Hence the specific heat does not diverge, but it peaks at a

Figure 2: Snapshots of the configuration at different values of the bending rigidity a) $\kappa = 0.5$, b) $\kappa = 0.8$ c) $\kappa = 1.1$. The different sizes indicate how R_g varies with κ.

value of κ close to its infinite volume limit κ_c. Both the height of the peak and its position scale with system size. Under general assumptions one can use finite size scaling to extract the critical exponent α from the measurements at finite volume. In Figure 1 we show the measured specific heat for surfaces of size 16^2–64^2. Our data, still preliminary in this region of the phase diagram, give $\alpha = 0.4(1)$ which is consistent with estimates from previous numerical simulations[10] ($\alpha = 0.58(10)$.)

4.2 The radius of gyration

The second observable we measure is the radius of gyration, or the linear extent of the surface,

$$R_g^2 = \frac{1}{N} \left\langle \sum_i \mathbf{n}_i \cdot \mathbf{n}_i \right\rangle. \tag{10}$$

As the system goes trough the crumpling transition the surface increases in size. This is reflected in R_g, which changes dramatically both in its actual value and its scaling. The scaling of R_g with the system size N defines the

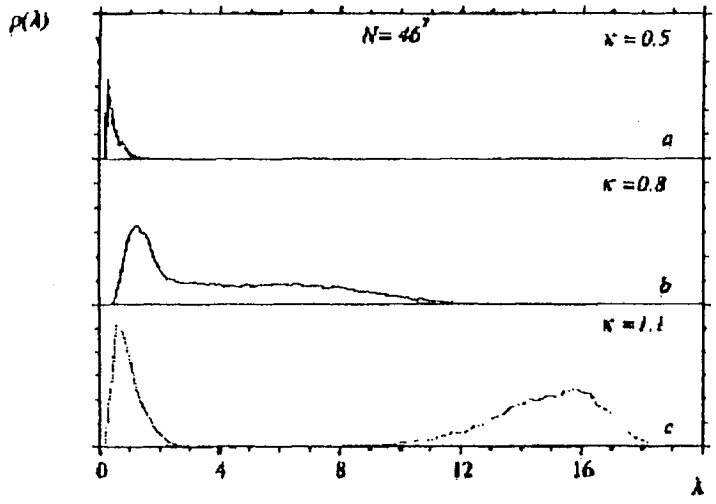

Figure 3: The distribution of eigenvalues $\rho(\lambda)$ of the inertia tensor.

Hausdorff dimension d_H of the surface

$$R_g \sim N^{1/d_H}. \tag{11}$$

The crumpled phase $\kappa < \kappa_c$ (see Figure 2a) is characterized by very small R_g. Also R_g does not seem to scale with system size according to a power law. It can be shown that at $\kappa = 0$ R_g scales as $\log(N)$, which implies $d_H = \infty$. In the flat phase (see Figure 2c) R_g is large and it scales linearly with system size. Fitting Eq. (11) to our data gives a Hausdorff dimension $d_H = 2.1(1)$. In the critical region the Hausdorff dimension has a non-trivial intermediate value. Earlier numerical work[6] indicates that $d_H = 4$ at κ_c (see Figure 2b).

4.3 The inertia tensor

The eigenvalues of the inertia tensor, related to the radius of gyration, also provide useful information about the phase diagram of this model. The inertia tensor

$$I_{\alpha\beta} = \delta_{\alpha\beta}(\mathbf{r}_\gamma)^2 - \mathbf{r}_\alpha \mathbf{r}_\beta = \delta_{\alpha\beta}(\mathbf{r}_\gamma)^2 - S_{\alpha\beta} \tag{12}$$

has an isotropic part—which scales like R_g^2, and an anisotropic part $S_{\alpha\beta}$, often called the *shape tensor*. The three eigenvalues of $S_{\alpha\beta}$ are the average square fluctuation of the surface in the directions of the corresponding eigenvectors.

The eigenvectors define a body-fixed frame which fluctuates along with the surface. We measure the eigenvalues by diagonalizing $S_{\alpha\beta}$ for each configuration of the Monte Carlo sequence.

The distribution ρ of these eigenvalues is very interesting. In the crumpled (high temperature) phase we expect the surface to be isotropic (symmetric under $O(3)$ rotations). This can be seen in Figure 3a, as the ρ has a single peak. In the critical region the distribution ρ still has a single peak: the system is still isotropic. Nonetheless we observe a long tail towards larger values of the eigenvalues (Figure 3b), a feature which we attribute to increasing fluctuations. In the flat phase the distribution has two well resolved peaks: the $O(3)$ symmetry is broken (Figure 3c). The left peak corresponds to the average square thickness of the surface, say, in the $\hat{z}$ direction, while the peak to the right corresponds to the lateral square size of the surface in the $\hat{x}$ and $\hat{y}$ directions. We cannot resolve the $\hat{x}$ and $\hat{y}$ directions, hence there is a left-over $O(2)$ symmetry in the surface, corresponding to rotations about the $\hat{z}$ axis.

5 The Flat Phase

In the flat phase we analyze observables which we compare to predictions from the continuous model Eq. (1). In particular we measure the anomalous scaling dimension of the bending rigidity κ_R, using the finite size scaling of the integrated height-height correlation function.[15] This scaling defines the *roughness exponent* ζ,

$$\langle h^2 \rangle \sim L^{2\zeta}, \tag{13}$$

which is related to the anomalous dimension η of Eq. (4) by

$$\eta = 2(1-\zeta). \tag{14}$$

To measure this correlation function we look at the average square thickness of the surface, defined by the minimum eigenvalue of the shape tensor. This quantity is well defined only in the flat phase. A careful analysis of data collected for sizes $L = 32$, 46, 64, and 128 at $\kappa = 1.1$ gives $\zeta = 0.64(2)$. Particular care has to be given to the effect of the free boundary on the data.[15] This value can be compared to analytical results, $\zeta = 0.590$[13] and $\zeta = 2/3$,[11] experiments on the spectrin of red blood cells, $\zeta = 0.65(10)$.[4] Previous numerical investigations on tethered models of surfaces have found values in the range 0.5–0.7 (see[15] for a full list of references).

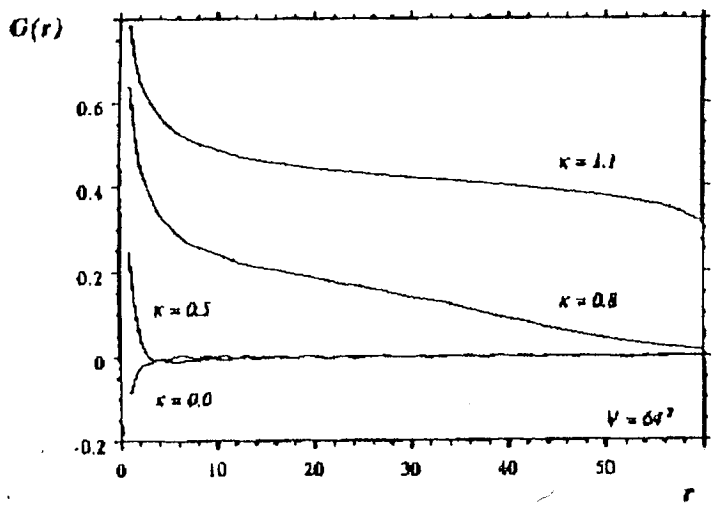

Figure 4: The normal-normal correlation for various values of the bending rigidity κ.

5.1 *The phonon fluctuations and the normal-normal correlation function*

There are two independent check of this estimate. We have measured the anomalous scaling of the elastic constants from the finite size scaling of the *phonon fluctuations*; $\langle |\mathbf{u}|^2 \rangle \sim L^{\eta_u}$. The exponent η_u is related to η through $\eta = 1 - \eta_u/2$. Our data for the phonon fluctuation at $\kappa = 1.1$ gives $\eta_u = 0.50(1)$. This implies $\eta \simeq 0.75$, in agreement with the value of η obtained from ζ. Finally, we measured the normal-normal correlation function, i.e. the average of the dot product between normals to the surface, separated by a geodesic distance r:

$$G(r) = \langle \mathbf{n}_o \cdot \mathbf{n}_r \rangle. \tag{15}$$

Since we consider surfaces with free boundaries it is not translationally invariant. To minimize boundary effects in the measurement we only consider correlations from the center o to points at distance r.

The normal-normal correlation has a distinguished behavior in the different phases (see Figure 4.) In the crumpled phase the correlation is *negative*, implying that even neighboring triangles are, on average, at angles greater than $\pi/2$. At the crumpling transition $G(r)$ decays to zero algebraically with a positive exponent related to the Hausdorff dimension d_H.[5] In the flat phase $G(r)$ approaches a *non-zero* asymptote as

$$\langle \mathbf{n}_o \cdot \mathbf{n}_o \rangle \approx C + \frac{c}{r^\eta}. \tag{16}$$

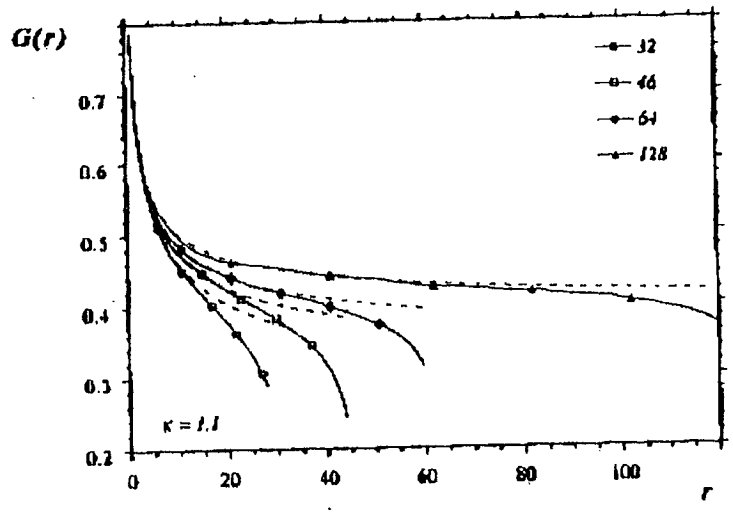

Figure 5: The normal-normal correlation for $\kappa = 1.1$ and various values of the lattice size.

This implies that the surface is asymptotically flat and stable against fluctuations. We have measured the normal-normal correlation $G(r)$ in the flat phase ($\kappa = 1.1$) and we show the results in Figure 5. From the figure it is clear that the small lattices are not sufficient to clearly see a non-zero asymptote for $G(r)$, while the asymptote stabilizes well for $L = 64$ and $L = 128$. This justifies our efforts to push the simulations to very large lattices, even though it required 6 months of running on a massively parallel computer. The exponent with which the correlation decays is, again, η. A careful analysis of the correlation gives a value of $\eta = 0.62$, and $C = 0.45$ for the asymptote. This is in quantitative agreement with the other estimates.

6 Conclusions

In the work we presented here we have shown that the very simple model of a crystalline surface Eq. (5) indeed has stable flat phase. The scaling exponents measured in this phase agree with the analytical predictions, experiments and previous numerical work. For completeness we have also investigated the model around the critical point. This work is still in progress but we expect to measure the critical exponents governing the crumpling transition with great accuracy.

Acknowledgments

David Nelson has contributed to this work with many suggestions and comments. We would also like to thank Mehran Kardar, Emmanuel Guitter, Alan Middleton, Paul Coddington and Gerard Jungman for helpful discussions. The research of MB and MF was supported by the Department of Energy U.S.A. under contract No. DE-FG02-85ER40237. SC and GT were supported by research funds from Syracuse University. Part of the work of KA was done at the Institute for Fundamental Theory at Gainesville and was supported by DOE grant No. DE-FG05-86ER-40272.

References

1. D. R. Nelson and L. Peliti in *Fluctuating Geometries in Statistical Mechanics and Field Theory*, edited by P. Ginsparg, F. David, and J. Zinn-Justin (cond-mat/9502114 or http://xxx.lanl.gov/lh94/, Les Houches, France, 1994), lectures given at the Les Houches Summer School.
2. X. Wen *et al.*, Nature 355, 426 (1992).
   T. Hwa, E. Kokufuta, and T. Tanaka, Phys. Rev. A 44, R2235 (1991).
3. R. R. Chianelli, E. B. Prestridge, T. Pecoraro, and J. P. DeNeufville, Science 203, 1105 (1979).
4. C. F. Schmidt *et al.*, Science 259, 952 (1993).
5. Y. Kantor and D. Nelson, Phys. Rev. Lett. 58, 2774 (1987).
6. J. Ambjørn, B. Durhuus, and T. Jonsson, Nucl. Phys. B 316, 526 (1989).
7. A. Polyakov, Nucl. Phys. B 268, 406 (1986).
8. R. Harnish and J. Wheater, Nucl. Phys. B 350, 861 (1991).
9. M. Baig, D. Espriu, and A. Travesset, Nucl. Phys. B 426, 575 (1994).
10. J. Wheater, Nucl. Phys. B 458, 671 (1996).
11. F. David and E. Guitter, Europhys. Lett. 5 (8), 709 (1988).
12. P. Le Doussal and L. Radzihovsky, Phys. Rev. Lett 69, 1209 (1992).
13. J. Aronovitz and T. Lubensky, Phys. Rev. Lett. 60, 2634 (1988).
14. E. Guitter, F. David, S. Leibler, and L. Peliti, Phys. Rev. Lett. 61, 2949 (1988).
15. K. Anagnostopoulos, M. Bowick, S. Catterall, M. Falcioni and G. Thorleifsson, cond-mat/9603157, to appear in J. Phys (France) October 1996.

GAUGE DEPENDENCE OF TOPOLOGICAL OBSERVABLES IN CHERN-SIMONS THEORY

F.A. DILKES, L.C. MARTIN, D.G.C. MCKEON
Department of Applied Mathematics
University of Western Ontario
London CANADA N6A 5B7

T.N. SHERRY
Department of Mathematical Physics
University College Galway
Galway IRELAND

We compute the one-loop contribution to the modulus of the effective action in pure non-Abelian Chern-Simons theory in an arbitrary covariant gauge. We find that the results depend on both the gauge parameter α and the metric required in the gauge fixing. A term of the form $(\alpha/\sqrt{p^2})\epsilon_{\mu\lambda\nu}p^\lambda$ arises which has not been previously encountered. This is possible as in three dimensions α is dimensionful. A variant of proper time regularization is used to render these integrals well behaved. Since the original Lagrangian is unaltered in this approach, no symmetries of the classical theory are explicitly broken and $\epsilon_{\mu\lambda\nu}$ is handled unambiguously since the system is three dimensional at all stages of the calculation. The results are shown to be consistent with the Nielsen identities which predict the explicit α dependence using an extension of BRS symmetry. We demonstrate that this α dependence may potentially contribute to the expectation values of products of Wilson loops.

1 Introduction

Non-Abelian Chern-Simons theory is an example of a three-dimensional topological theory. It has been argued that radiative corrections in the theory serve only to displace the coupling constant, despite the fact that the gauge fixing term that must be appended to the classical Lagrangian is metric dependent.[1] This is consistent with a number of (but not all) perturbative calculations, each of which requires some form of regularization.[2-9] Regulating this model is complicated by the three dimensional nature of the tensor $\epsilon_{\alpha\beta\gamma}$ occurring in the initial Lagrangian, and by the fact that the theory is topological - it is difficult to respect these properties if one regulates by altering the initial Lagrangian in some way. (For example, addition of a Yang-Mills term to the Chern-Simons Lagrangian[3,5,8] does not respect its topological nature and simple Pauli-Villars regularization[2] breaks BRS invariance.[6]) A way of circumventing this difficulty is to use a variant of operator regularization.[10]

At one loop order, one encounters a functional determinant $\det M$. Since